

Advanced Measurements of Silicon Carbide Ceramic Matrix Composites

David Hurley
Farhad Fazbod
Zilong Hua
Stephen Reese
Marat Khafizov

August 2012



The INL is a U.S. Department of Energy National Laboratory
operated by Battelle Energy Alliance

DISCLAIMER

This information was prepared as an account of work sponsored by an agency of the U.S. Government. Neither the U.S. Government nor any agency thereof, nor any of their employees, makes any warranty, expressed or implied, or assumes any legal liability or responsibility for the accuracy, completeness, or usefulness, of any information, apparatus, product, or process disclosed, or represents that its use would not infringe privately owned rights. References herein to any specific commercial product, process, or service by trade name, trade mark, manufacturer, or otherwise, does not necessarily constitute or imply its endorsement, recommendation, or favoring by the U.S. Government or any agency thereof. The views and opinions of authors expressed herein do not necessarily state or reflect those of the U.S. Government or any agency thereof.

Advanced Measurements of Silicon Carbide Ceramic Matrix Composites

**David Hurley
Farhad Farzbod
Zilong Hua
Stephen Reese
Marat Khafizov**

August, 2012

**Idaho National Laboratory
Materials Science and Engineering Department
Idaho Falls, Idaho 83415**

<http://www.inl.gov>

**Prepared for the
U.S. Department of Energy
Office of Nuclear Energy
Under DOE Idaho Operations Office
Contract DE-AC07-05ID14517**

ABSTRACT

Silicon carbide (SiC) is being considered as a fuel cladding material for accident tolerant fuel under the Light Water Reactor Sustainability (LWRS) Program sponsored by the Nuclear Energy Division of the Department of Energy. Silicon carbide has many potential advantages over traditional zirconium based cladding systems. These include high melting point, low susceptibility to corrosion, and low degradation of mechanical properties under neutron irradiation. In addition, ceramic matrix composites (CMCs) made from SiC have high mechanical toughness enabling these materials to withstand thermal and mechanical shock loading.

However, many of the fundamental mechanical and thermal properties of SiC CMCs depend strongly on the fabrication process. As a result, extrapolating current materials science databases for these composite materials to nuclear applications is not possible. The “Advanced Measurements” work package under the LWRS fuels pathway is tasked with the development of measurement techniques that can characterize fundamental thermal and mechanical properties of SiC CMCs. An emphasis is being placed on development of characterization tools that can be used for examination of fresh as well as irradiated samples.

The work discussed in this report can be divided into two broad categories. The first involves the development of laser ultrasonic techniques to measure the elastic and yield properties and the second involves the development of laser-based techniques to measure thermal transport properties. Emphasis has been placed on understanding the anisotropic and heterogeneous nature of SiC CMCs in regards to thermal and mechanical properties. The material properties characterized within this work package will be used as validation of advanced materials physics models developed under the LWRS fuels pathway. In addition, it is envisioned that similar measurement techniques can be used to provide process control and quality assurance as well as measurement of in-service degradation. Examples include composite density, distribution of porosity, fiber-matrix bond character, uniformity of weave, physical damage, and joint quality at interface bonds.

CONTENTS

ABSTRACT	iv
ACRONYMS	vi
1. Introduction	1
2. Sample Specifications	1
3. Mechanical Properties Measurements	2
3.1 Elastic Properties.....	2
3.1.1 Cantilever beam theory	3
3.1.2 Relation between symmetry and fiber layup.....	4
3.1.3 Preliminary measurements of elastic properties of SiC CMC	5
3.2 Yield Properties.....	6
4. Thermal Properties Measurements	7
5. Conclusion.....	8
6. References	9

ACRONYMS

CMC	Ceramic matrix composite
CVI	Chemical vapor infiltration
INL	Idaho National Laboratory
LRUS	Laser resonance ultrasound spectroscopy
MTR	Modulated thermorefectance
ORNL	Oak Ridge National Laboratory
RUS	Resonant ultrasound spectroscopy
SiC	Silicon carbide

Error! Reference source not found.

1. Introduction

The physical properties of ceramics and ceramic based composite materials are strongly tied to microstructure. For monolithic ceramics, pores and micron size cracks will influence both mechanical and thermal properties. For fiber-based composite materials the bond between fiber and matrix plays an important role in overall performance. To assist in the design and deployment of new ceramic based fuel cladding materials there is need for a characterization approach that relates the fundamental response of the constituents to the overall performance of the composite. This approach will provide valuable information to help refine fabrication technologies and will provide critical input data and validation metrics for computational materials science models. In addition, many of the characterization tools are non-destructive in nature and may be suitable for future quality and process control measurements.

There are many challenges related to the characterization of physical properties of ceramic based cladding materials. Silicon carbide (SiC) ceramic matrix composites (CMC) are a leading candidate for advance cladding materials and provide an illustrative example of the challenges related to materials characterization. CMCs are heterogeneous and anisotropic. As a result the measurement of thermo-mechanical properties depends on length scale and direction.

In this document we report on progress towards measuring the fundamental elastic and thermal properties of baseline SiC CMC samples. Resonant ultrasound experiments were conducted to probe the elastic response of the material. The preliminary results indicate that the material has a strong elastic anisotropy. We also measured the thermal response using laser flash and thermal wave imaging. The preliminary results indicate that the matrix material has a reduced thermal diffusivity in comparison to monolithic SiC.

2. Sample Specifications

The baseline sample consisted of a dog bone shaped sample derived from a flat CMC plate fabricated by Hyper-Therm, Inc. for Oak Ridge National Laboratory (ORNL). The samples were provided to the INL through an informal collaboration between William Windes at INL and Yutai Katoh at ORNL. The material was processed with chemical vapor infiltration (CVI) conditions that targeted a fiber coating composed of (150 nm pyrolytic carbon, (100 nm CVI SiC, 20 nm pyrolytic carbon)) and subsequently densified with CVI SiC. The CVI SiC is crystalline with a cubic structure and a density of 3.2 g/cm^3 . The fiber used for fabrication is stoichiometric Nicalon Type S fiber. The measured biaxial braid angle is 55° and the number of braid layers is 10. The fiber volume is estimated to be nominally 30%. The plate

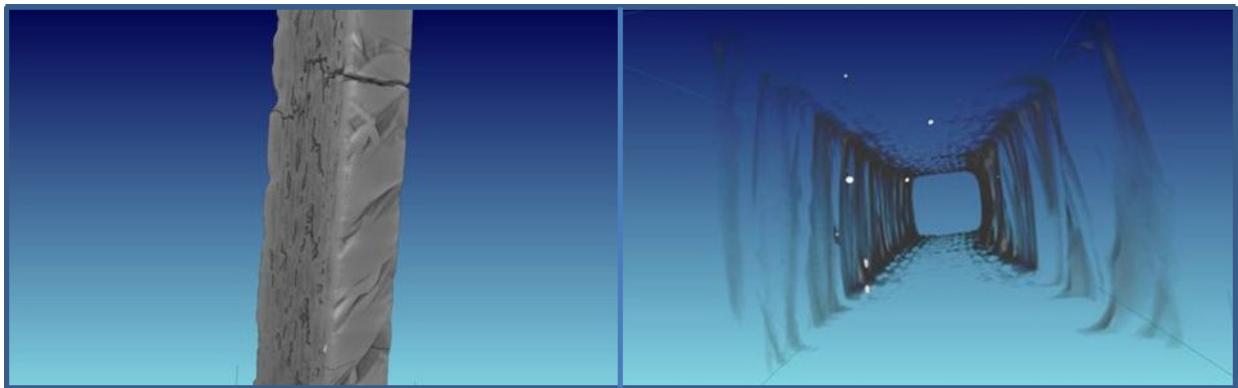


Figure 1. X-ray tomographic images of SiC CMC sample. Left: Surface rendering of cracked region. Right: Volume rendering that reveals the presence of inclusions (visible as white dots in the image).

thickness was approximately 2.9 mm prior to the application of a thick seal coat. The purpose of the seal

coat is to allow machining without machining fiber. Several long narrow test specimens were cut from the baseline sample. These test specimens were used in flexural tests and resonant ultrasound tests.

Before conducting detailed elastic and thermal property characterization it is important to characterize the bulk density and fiber distribution in the composite sample. Poorly fabricated samples having large areas of high porosity should be avoided. To this end we have analyzed our specimen using X-ray tomography. The microfocus X-ray system uses a Hamamatsu 130kV, 0.3mA source and a Varian PaxScan 2520 detector. The system's maximum magnification is 30 \times and its ultimate resolution is approximately 4 μ m.

An X-ray micrograph of the typical test specimen is shown in left pane of Fig. 1. This particular test specimen was used in a flexural test that was run to failure. The dominant crack running across the sample is clearly evident. Because the density of the matrix and the fiber are similar it is difficult to distinguish the fiber from the matrix. However, the stacking sequence is clearly observable from the surface topography. By using gray scale analysis this X-ray micrograph can be used to determine the local density of the composite material. In addition to vetting samples prior to characterization, this would be a key piece of information used to resolve anomalous non-destructive characterization data. A volume rendering is shown in the right pane of Fig. 1. This image reveals the presence of inclusions likely introduced during the fabrication process. Depending on size, chemistry and distribution, these inclusions may play an important role in limiting the mechanical performance of SiC cladding systems.

3. Mechanical Properties Measurements

The mechanical performance of a SiC CMC is defined in large part by the specific fiber weave and the interaction of fibers with the matrix. The fibers introduce directionality to the CMC causing the elastic properties to become direction dependent (elastic anisotropy). The nature of the elastic anisotropy will depend strongly on the fiber weave.^{1,2} The yield properties and fracture strength of the CMC are determined by the bond between the fiber and matrix. Typically a thin carbon coating is added to the surface of the fiber to allow for a moderate amount of fiber pullout during deformation. CMCs are engineered so that the optimal fracture toughness typically corresponds to a total elongation of 0.05 - 0.2%. Thus, the 0.2% yield strength commonly used with metals may not be appropriate for brittle ceramic composites. A more appropriate measurement of the yield properties is the proportional limit which is characterized by the onset of microcracking in the matrix.³

3.1 Elastic Properties

The elastic constants of a material relate strain to stress. For isotropic materials there are two independent elastic constants, typically given as Young's modulus and the shear modulus. For some materials (e.g. single crystals, textured polycrystals and fiber composites) the elastic properties are a function of the direction in which they are measured. These materials are referred to as elastically anisotropic. Understanding the extent and direction of elastic anisotropy is crucial for correctly predicting the stress-displacement behavior of fuel assemblies. For example in nuclear fuel assemblies, stress displacement behavior is critical to understanding the onset of fuel cladding chemical interaction.

Traditionally these constants have been obtained using load frame tests. However for elastically anisotropic materials such as SiC CMC, load frame tests can only give very limited data on elastic anisotropy. This is because load frames are not well suited to measure out-of-plane anisotropy because of minimum sample size limitations.

The elastic constants can also be measured using ultrasonic techniques. This approach typically uses piezoelectric transducers to measure the longitudinal and shear acoustic wave velocities. By accurately measuring the propagation distance, one is able to recover Young's modulus and the shear modulus. For elastically anisotropic materials, all of the elastic constants can be recovered by cutting many samples having different orientations relative to the principle symmetry axes of the sample. However, it should be noted that distinguishing the various wave arrivals in an anisotropic material can be a daunting task. For

heterogeneous samples such as fiber reinforced composites, identifying wave arrivals is further complicated by multiple reflections from internal boundaries and interfaces. For these materials it is preferable to use long wavelength acoustic waves that are resonant with the sample. The scattering strength of the internal boundaries drops dramatically with increasing acoustic wavelength. Thus, for long wavelengths the material takes on the character of a homogeneous continuum. This approach is termed resonant ultrasound spectroscopy (RUS).

3.1.1 Cantilever beam theory

The natural frequency of vibrating beams has been used as a means of determining the elastic properties of materials. Numerous standards exist detailing such measurements.^{4,5,6} The resonant frequency depends only on the beam geometry, density, and elastic properties. The use of free-free beams is generally specified in these standards in order to minimize boundary condition errors associated with the clamping and pinning of beams in other configurations.⁷ However, cantilever beams offer advantages for measurements of materials in harsh environments (e.g. temperature, radiation) in that the beams can be rigidly held in position and alignment with the detection system maintained. By carefully controlling the beam clamping and using an indexing holder, the errors associate with the clamped boundary condition can be minimized.

In order to make this measurement technique robust, it is required to have a theory capable of predicting the eigenfrequencies and eigenmodes of higher order modes. One compelling reason for this requirement, discussed in detail in a subsequent section, is that the practitioner must be able to correctly identify modes. Unambiguous mode identification enables an accurate measurement of the elastic constants and is especially important for elastically anisotropic materials.

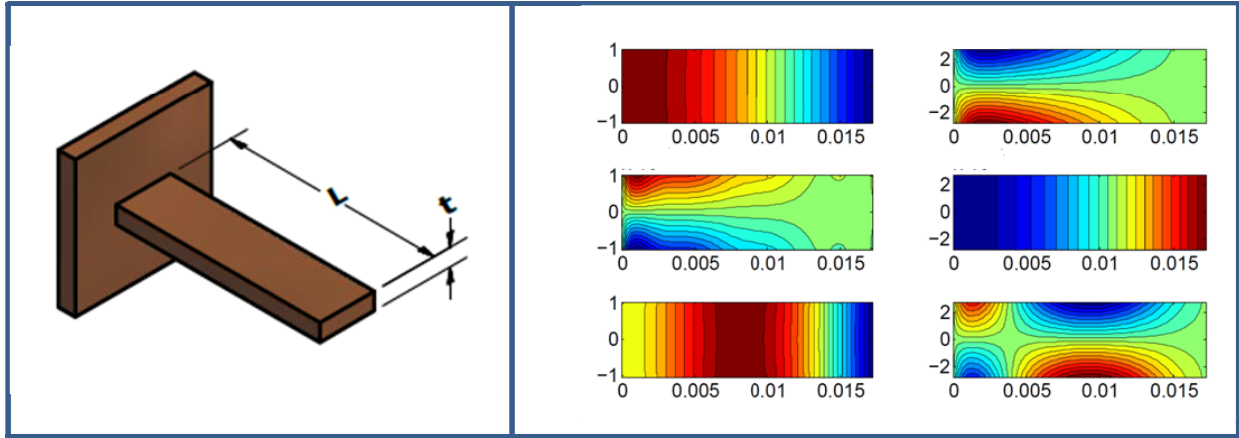


Figure 2. Left: bar geometry. Right: From left to right, the first six eigenmodes. The higher order flexural and torsional modes are clearly evident.

Towards this end we have developed a theoretical technique, based on the Ritz method, to calculate eigenfrequencies and eigenmodes of a cantilever beam. This is an exact treatment of the problem, and as such, does not resort to making assumptions regarding shear deformation or rotary inertia. This method has the advantage of determining eigenmodes as well as eigenfrequencies and is based on a previous development for free-free beams.⁸ The problem geometry is shown on the left side of Fig. 2. The bar length is L and the thickness is t . The first six eigenmodes are shown in the right side of Fig. 2. The first, fourth, and fifth modes correspond to flexural modes. The second and sixth modes correspond to torsional modes. We have compared this new model against the Euler-Bernoulli theory for long thin bars. For this comparison we considered a cantilever beam cut from a highly textured copper sample ($C_{1111} = 174$ GPa, $C_{1122} = 118$ GPa, and $C_{2323} = 65$ GPa).⁹ Note that here we are using the elastic stiffness tensor to relate stress to strain for an anisotropic material. The eigenvalue problem was solved numerically for various cantilever beam lengths. (The width, 0.5

mm, and the thickness, 2 mm, were fixed.) Eigenfrequencies are tabulated in Table1 and are compared to the Euler-Bernoulli theory. As is evident in the table, Euler-Bernoulli theory approaches the exact theory as the bar length increases.

Table 1. Eigenfrequencies for various beam lengths with 2×5 mm rectangular cross-section. Frequencies are calculated by Euler-Bernoulli formalism and a numerical solution to the exact problem (denoted EP).

5 mm		15 mm		25 mm		50 mm	
EP method (Hz)	Euler-Bern. (Hz)	EP method (Hz)	Euler-Bern. (Hz)	EP method (Hz)	Euler-Bern. (Hz)	EP method (Hz)	Euler-Bern. (Hz)
10035	9603	1094	1067	391	384	97	96
36788		4292		1550		388	
60907	60182	6833	6687	2451	2407	610	602
64116		19103	18723	6863	6740	1710	1685
ij151204	168511	20551		9553		2422	
164859		25695		12231		3353	3303
172714		37384	36695	13458	13210	5549	5459

3.1.2 Relation between symmetry and fiber layup

As was alluded to in the previous section, the elastic properties of anisotropic materials are most conveniently given using tensor notation. Relating stress, σ_{ij} , to strain, ϵ_{kl} , involves the stiffness tensor (C_{ijkl}) and relating strain to stress involves the compliance tensor (S_{ijkl}). Typically, the matrix representation of these tensors is used to aid in bookkeeping. The matrix representation involves replacing the first and second pairs of subscripts (ij and kl, respectively) with a single subscript running from 1 to 6, as is shown here for the stiffness matrix:

$$\begin{pmatrix} \sigma_1 \\ \sigma_2 \\ \sigma_3 \\ \sigma_4 \\ \sigma_5 \\ \sigma_6 \end{pmatrix} = \begin{pmatrix} C_{11} & C_{12} & C_{13} & C_{14} & C_{15} & C_{16} \\ C_{21} & C_{22} & C_{23} & C_{24} & C_{25} & C_{26} \\ C_{31} & C_{32} & C_{33} & C_{34} & C_{35} & C_{36} \\ C_{41} & C_{42} & C_{43} & C_{44} & C_{45} & C_{46} \\ C_{51} & C_{52} & C_{53} & C_{54} & C_{55} & C_{56} \\ C_{61} & C_{62} & C_{63} & C_{64} & C_{65} & C_{66} \end{pmatrix} \begin{pmatrix} \epsilon_1 \\ \epsilon_2 \\ \epsilon_3 \\ \epsilon_4 \\ \epsilon_5 \\ \epsilon_6 \end{pmatrix}$$

A similar expression, using the compliance matrix, can be obtained for the relation between strain and stress.

Using energy arguments it can be shown that there are at most 21 independent elastic constants. Most materials have considerably fewer independent elastic constants. For instance, a single crystal cubic material such as copper has three independent elastic constants. For isotropic materials (e.g. polycrystal with random crystallite orientation) there are only two independent elastic constants. To put this in familiar terms for engineers, Young's modulus and the shear modulus for isotropic materials can be expressed in terms of the compliance matrix as follows:

$$E = \frac{1}{s_{11}}, \quad G = \frac{1}{2(s_{11} - s_{12})}.$$

The independent elastic constants for fiber composites can be found in much the same way as single crystals. The method involves application of Neumann's principle which states that the tensor property must include the same symmetry elements as the fiber composite. As an example, consider a unidirectional fiber composite. If we assume maximum staking density of fibers (i.e. hexagonal

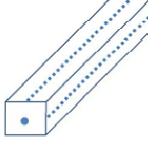
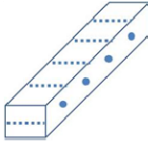
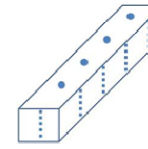
Ply orientation / Stacking order	Symmetry	Independent elastic constants	Elastic constants relations	# of elastic constants that can be measured	
Unidirectional	Hexagonal (transversely isotropic)	5	$S_{11}=S_{22}$ $S_{13}=S_{23}$ $S_{44}=S_{55}$ $S_{66}=2(S_{11}-S_{12})$	4 (S_{11} , S_{33} , S_{44} , S_{12})	 Flexural mode – S_{11} Torsional mode – S_{66}
(0/90) _s	Tetragonal	6	$S_{11}=S_{22}$ $S_{13}=S_{23}$ $S_{44}=S_{55}$	3 (S_{11} , $2S_{12}+S_{66}$, S_{44})	 Flexural mode – S_{33} Torsional mode – S_{44}
(60/0/-60) _s , (0/45/-45/90) _s	Hexagonal (transversely isotropic)	5	$S_{11}=S_{22}$ $S_{13}=S_{23}$ $S_{44}=S_{55}$ $S_{66}=2(S_{11}-S_{12})$	2 (S_{11} , S_{44})	 Flexural mode – S_{33} Torsional mode – S_{66}
(0/55) ₃ orthogonal mirror planes	Orthorhombic	9	NA	5 (S_{11} , S_{22} , $2S_{12}+S_{66}$, S_{44} , S_{55})	

Figure 3. Left: Table listing the fiber layout and the corresponding independent elastic constants. Right: Schematic showing the elastic constants that can be measured and the corresponding fiber direction relative to the beam axis.

arrangement) then the material will possess one 6-fold axis of symmetry that is parallel to the fibers. For this material there are five independent elastic constants. On the left side of Fig. 3 a table is presented that lists common fiber layouts and the number of independent elastic constants.

The question remains as to how many of these constants can be extracted using ASTM standards for measurement of dynamic elastic constants. These standards involve application of the vibrating beam technique to measure flexural and torsional resonant frequencies. These frequencies can be used to extract the elastic constants. Again using unidirectional fiber composites as an example, S_{11} and S_{66} can be measured from the flexural and torsional modes for the case where the fibers are along the axis of the beam. More constants can be measured if the fiber orientation relative to the beam axis can be changed. This may or may not be possible depending on the sample from which the beams are derived. A schematic showing which elastic constants can be measured along with fiber orientation relative to the beam axis is shown on the right of Fig. 3.

3.1.3 Preliminary measurements of elastic properties of SiC CMC

The elastic properties of our CMC baseline sample were made using time domain laser ultrasound and frequency domain laser resonance ultrasound spectroscopy (LRUS). Time domain ultrasound uses acoustic frequencies in the 100 MHz range and is not well suited to measure elastic properties of the composite. However, the spatial resolution of time domain ultrasound, $\sim 100 \mu\text{m}$, makes possible measurement of the elastic properties of the matrix material. This parameter is of particular relevance to continuum based finite element models of the mechanical response of SiC composites.

In the left pane of Fig. 4 the results of a time domain laser ultrasound study are presented. The experimental geometry involved generating acoustic waves on one surface and detecting the acoustic wave along the epicentral direction on the opposite face. The first wave arrival corresponds to the longitudinal wave and can be used to determine the longitudinal modulus ($\lambda+2\mu$). The value obtained for the matrix material in our baseline sample is 420 GPa.

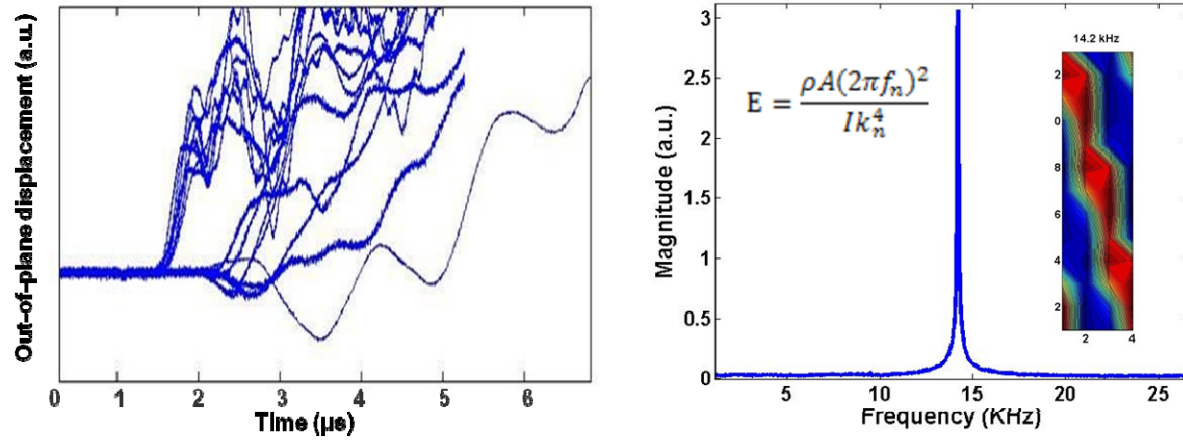


Figure 4. Results from a time domain study. Right: Results from a frequency domain study. The full color inset in the right pane shows the eigenmode corresponding to the third flexural mode.

Our frequency domain study involved exciting and detecting flexural vibrations in a free-free beam. In this case we excite broadband resonances in the beam with a pulsed laser and measure the ultrasonic ringdown with a laser interferometer. The frequency spectrum is obtained by taking the Fourier transform of the ringdown data. A typical resonance spectrum is shown in the right pane of Fig. 4. By raster scanning our probe we can get an image of the eigenmode corresponding to this eigenfrequency. The mode shape is shown in the inset. There are two points to note here. First, this mode is not the fundamental flexural mode but rather an overtone. A clear indication of the mode order number is critical to correctly extracting the elastic constants. Second, the mode shape lacks symmetry about the principle axes of the beam. This results from the fiber layup of this particular sample. As was stated in the sample specification section, the fiber layup is (0/55). A material with this fiber layup only possesses three orthogonal planes of mirror symmetry. As a result there are nine independent elastic constants. Moreover, a material with this symmetry does not have an axis of 4-fold symmetry. We recently presented a similar result for a rotated single crystal cubic material.¹⁰ In this work we showed that eigenmodes corresponding to a rotated single crystal lack symmetry about the principle axes of the sample.

3.2 Yield Properties

As point out by Snead and coworkers at ORNL, a more appropriate “yield” strength for ceramic matrix composites is the proportional stress limit. However, the location of the proportional limit is subject to relatively large experimental uncertainty. In this section we investigate determination of the proportional limit using a laser ultrasonic technique. The proportional limit in brittle CMC materials is indicated by the onset of micro-cracking in the matrix.

The presence of these micro-cracks leads to a measurable increase in acoustic attenuation. This point is illustrated in the left pane of Fig. 5. Here we have measured the resonant response of a sample before and after shock loading. Acoustic attenuation is related to the width of the peak or the quality factor. Low attenuation corresponds to a high quality factor. After shock loading, the quality factor decreased by approximately 30%. This decrease in quality factor is in keeping with the presence of micro-cracking in the matrix as indicated by the optical microscope image of the sample shown in the inset of the left pane of Fig. 5. This image reveals cracks in the matrix material that have been blunted or arrested upon encountering a fiber.

To test whether we could see similar changes during loading we instrumented a load frame with a laser ultrasound apparatus. The results of this study are shown on the right side of Fig. 5. The instrumented bend test is shown in the inset. Because the load frame contacts cause considerable coupling to the environment, the resonant peaks shift significantly during the test. As a result, we

currently are unable to track an individual resonant peak through the entire test. Instead we track the integrated power spectrum. This parameter gives us some estimate of the ultrasonic attenuation, but it is difficult to extract intrinsic attenuation from extrinsic attenuation caused by coupling to the environment (i.e., the contact force of the bending fixture contacts). By performing the test twice we can demonstrate that we are sensing the presence of damage in the matrix. The first test, shown in blue on the right of Fig. 5, is run to the proportional limit as indicated by the applied force strain curve. The second test is run to failure. We observe a permanent increase in attenuation that we attribute to damage incurred during the first run.

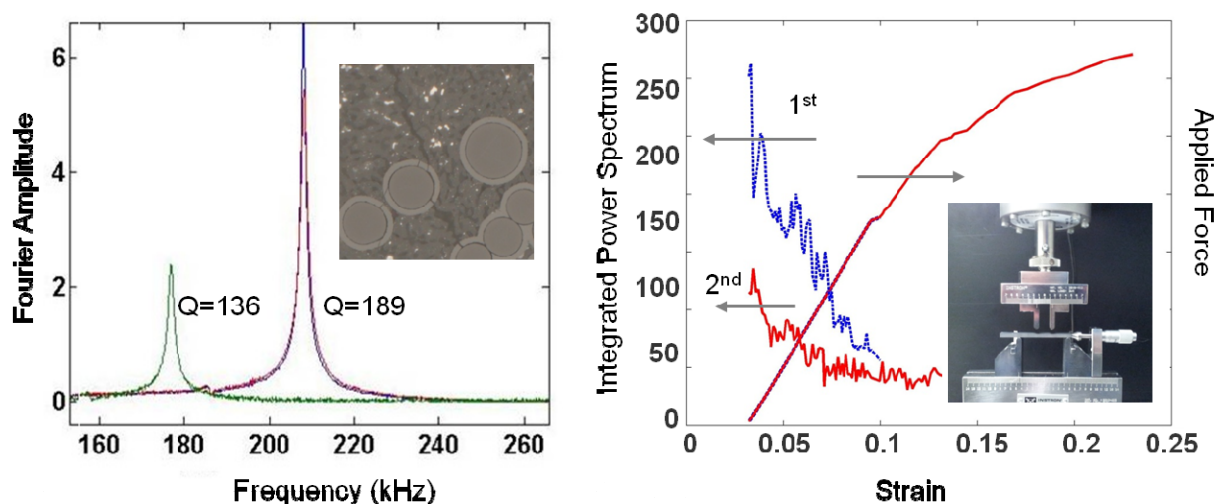


Figure 5. Left: Measuring ultrasonic attenuation in a shock loaded sample. Attenuation before (purple peak) and after shock loading (green peak) are shown. Right: Measuring ultrasonic attenuation during a load test.

4. Thermal Properties Measurements

Due to the scarcity of free electrons, thermal transport in ceramic materials is dominated by phonon transport. As a phonon conductor, the thermal conductivity of SiC is strongly influenced by neutron damage. This behavior is in contrast to metals where thermal energy is carried by free electrons. In metals, the influence of neutron damage on thermal transport is significantly less than in ceramics. Because thermal energy must be transported out of the fuel assembly in order to be converted into electricity, it is important to clearly understand the role of neutron damage on limiting thermal transport in SiC CMC.

For composite materials, one must consider the thermal properties of the matrix and fibers. SiC fibers, even stoichiometric fibers, have relatively low thermal conductivity compared to monolithic SiC. As a consequence, the matrix transports the majority of the thermal energy. Understanding the degradation of thermal conductivity in the matrix, especially at low temperature, is essential to understanding thermal transport in the composite material. Studying the degradation of monolithic SiC in a high radiation environment has provided much insight into the fundamental mechanisms that govern thermal transport; however, additional insight can be obtained by measuring the degradation of thermal conductivity in the matrix material of a composite. This approach will require a spatially resolved technique to probe thermal conductivity on micron scale spatial dimensions. To this end we investigate making spatially resolved measurements of thermal diffusivity in SiC composite materials. Our approach is based on generation and detection of thermal waves using amplitude modulated lasers. Termed modulated thermorefectance (MTR), this approach has been applied successfully to a wide range of materials, from insulators to thermal conductors.^{11,12}

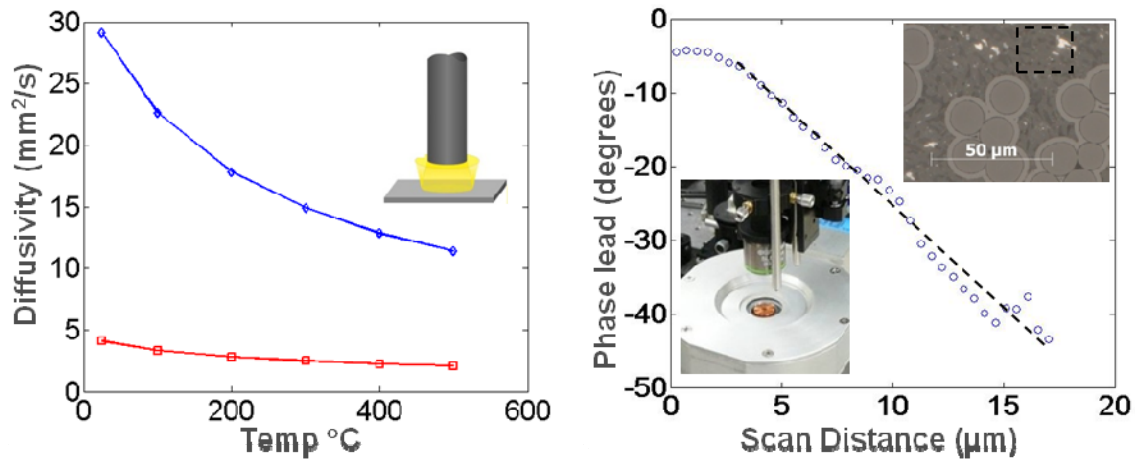


Figure 6. Left: Laser flash results for monolithic SiC (blue curve) and SiC CMC (red curve). Right: Spatially resolved MTR results on the matrix material of the CMC.

To initiate this study we performed baseline measurements using a laser flash apparatus located in the Carbon Laboratory at INL. The laser flash results are shown in the left pane of Fig. 6. We tested two samples – monolithic SiC and a SiC CMC composed of Nicalon Type S fibers. This particular CMC sample was obtained from John Garnier at INL and is not from our baseline CMC sample discussed in Sections 2 and 3. As expected, the monolithic SiC sample has a much larger thermal diffusivity than the CMC material.

In the right side of Fig. 6 we show results from our MTR study on the same CMC material used in the laser flash study. A close-up photograph of the sample environmental chamber and the microscope objective use to deliver both pump and probe laser beams is shown in the bottom inset on the right side of Fig. 6. The region probed ($\sim 20 \times 20 \mu\text{m}$) is shown in the dashed square in the upper inset in the right side of Fig. 6. The thermal wave phase versus scan distance gives a linear relationship in the far-field of the laser source. The slope of the phase profile in this region can be used to directly obtain thermal diffusivity. From this measurement, the thermal diffusivity of the matrix material is estimated to be $14.5 \text{ mm}^2/\text{s}$. This value is approximately in the middle between the room temperature values for the monolithic and CMC materials (see left pane of Fig. 6). Thus the relatively low value of the CMC diffusivity can be viewed as due to thermal resistance caused by the interface between the fiber and matrix as well as a reduced diffusivity of the matrix material in comparison to the monolithic sample.

5. Conclusion

The mechanical and thermal properties of baseline SiC CMC samples have been measured using laser-based techniques. Emphasis has been placed on understanding the anisotropic and heterogeneous nature of these materials. In the mechanical properties section of this report it was shown that the fiber weave of our baseline sample (0/55) resulted in an elastically anisotropic material having low symmetry. It was determined that this material has 9 independent elastic constants. A resonant bar technique was developed to measure a large subset of the elastic constants. In addition, a load frame was instrumented with a laser ultrasound apparatus to enable measurement of acoustic attenuation associated with micro-cracking. This approach is being explored as a means to identify the proportional limit indicated by the onset of micro-cracking in the matrix. In the thermal properties section of this report it was shown that the composite sample has a much lower thermal diffusivity than the monolithic sample. Spatially resolved laser-based thermal transport measurements revealed that the reduced thermal conductivity of the composite sample is partially due a reduced value the matrix diffusivity in contrast to the monolithic sample. Future work will involve applying these laser-based techniques to a larger selection of baseline samples including samples that have been fabricated with intentional flaws.

6. References

- ¹ D. H. Hurley, J. B. Spicer, Point-Source Representation for Laser-Generated Ultrasound in an Elastic Transversely Isotropic Half Space, *Journal of Applied Physics*, **86**, 3423 (1999).
- ² D. H. Hurley, J. B. Spicer, An Investigation of the Effects of Material Anisotropy and Heterogeneity on Pulsed, Laser-Generated Acoustic Signals, *Ultrasonics Ferroelectrics and Frequency Control*, **46**, 1387 (1999).
- ³ Y. Katoh, L. L. Sned, T. Nozawa, S. Kondo, J. T. Busby, *Journal of Nuclear Materials*, **403**, 48 (2010).
- ⁴ ASTM E1875-08, ASTM International, West Conshohocken, PA, 2008.
- ⁵ ASTM C747-93, ASTM International, West Conshohocken, PA, 1993.
- ⁶ ASTM C623-92, ASTM International, West Conshohocken, PA, 1992.
- ⁷ H.E. Rosinger and I.G. Ritchie, *J. of Testing and Evaluation*, **2**(3),131-138, (1974).
- ⁸ W. M. Visscher, *et al.*, *Journal of the Acoustical Society of America*, vol. 90, pp. 2154-2162, Oct 1991.
- ⁹ D. H. Hurley, *et al.*, "In situ laser-based resonant ultrasound measurements of microstructure mediated mechanical property evolution," *Journal of Applied Physics*, vol. 107, Mar 2010.
- ¹⁰ F. Farzbod and D. H. Hurley, IEEE transactions on ultrasonics ferroelectrics and frequency control, accepted for publication, July 2012.
- ¹¹ M. Khafizov, D. Hurley, Measurement of Thermal Transport Using Time-resolved Thermal Wave Microscopy, *Journal of Applied Physics*, **110**, 83525 (2011).
- ¹² D. H. Hurley, M. Khafizov, S. Shinde, Hurley, D. Measurement of Kapitza Resistance Across a Bicrystal Interface, *Journal of Applied Physics*, **109**, 83504 (2011).